# Tuning interfacial ferromagnetism in $LaNiO_3/CaMnO_3$ superlattices by stabilizing nonequilibrium crystal symmetry

C. L. Flint,[1,2] A. Vailionis,[2] H. Zhou,[3] H. Jang,[4] J.-S. Lee,[4] and Y. Suzuki[2,5]

[1]*Department of Materials Science and Engineering, Stanford University, Stanford, California 94305, USA*

[2]*Geballe Laboratory for Advanced Materials, Stanford University, Stanford, California 94305, USA*

[3]*Advanced Photon Source, Argonne National Laboratory, Argonne, Illinois 60439, USA*

[4]*Stanford Synchrotron Radiation Lightsource, SLAC National Accelerator Laboratory, Menlo Park, California 94025, USA*

[5]*Department of Applied Physics, Stanford University, Stanford, California 94305, USA*

(Received 12 May 2017; published 31 October 2017)

Perovskite oxide heterostructures offer an important path forward for stabilizing and controlling low-dimensional magnetism. One of the guiding design principles for these materials systems is octahedral connectivity. In superlattices composed of perovskites with different crystal symmetries, variation of the relative ratio of the constituent layers and the individual layer thicknesses gives rise to nonequilibrium crystal symmetries that, in turn, lead to unprecedented control of interfacial ferromagnetism. We have found that in superlattices of $CaMnO_3$ (CMO) and $LaNiO_3$ (LNO), interfacial ferromagnetism can be modulated by a factor of 3 depending on LNO and CMO layer thicknesses as well as their relative ratio. Such an effect is only possible due to the nonequilibrium crystal symmetries at the interfaces and can be understood in terms of the anisotropy of the exchange interactions and modifications in the interfacial Ni-O-Mn and Mn-O-Mn bond angles and lengths with increasing LNO layer thickness. These results demonstrate the potential of engineering nonequilibrium crystal symmetries in designing ferromagnetism.

DOI: 10.1103/PhysRevB.96.144438

## I. INTRODUCTION

Transition-metal perovskite oxides exhibit a wide range of ground states which are a manifestation of the delicate balance of the lattice, charge, and spin degrees of freedom in these materials. Competing interactions with similar energy scales mean that small perturbations, be they external fields, pressure, or other parameters, can give rise to large changes in magnetic and electronic properties. In a transition-metal perovskite oxide with the $ABO_3$ structure, $BO_6$ octahedra form building blocks, and their relative connectivity can dramatically change its properties. In bulk single crystals, high pressure has been used to substantially modify the ground states of some of these transition-metal perovskite oxides [1–5]. More recently, there have been theoretical studies indicating that stabilizing new crystal symmetries via octahedra rotation patterns in oxide heterostructures may give rise to unexpected emergent behavior [6,7]. For example, Rondinelli and Fennie have predicted ferroelectricity in cation-ordered $LaGaO_3/YGaO_3$ superlattices due to stabilization of unique octahedral rotation patterns [8].

Due to their enhanced experimental signal arising from an increased number of interfaces, superlattices are model systems for exploring interfacial electronic and magnetic phenomena that are driven by octahedral connectivity. In ferromagnetic systems such as $La_{0.7}Sr_{0.3}MnO_3/Eu_{0.7}Sr_{0.3}MnO_3$, $LaMnO_3/SrTiO_3$, and $La_{0.7}Sr_{0.3}MnO_3$, experimental studies have shown that the magnetic properties are tunable through interfacial $MnO_6$ octahedral tilt and rotation [9–12]. Grutter *et al.* have also attributed the suppression of emergent ferromagnetism in $CaRuO_3/CaMnO_3$ (CRO/CMO) superlattices to independent specific octahedral rotation orientations [13]. In these CRO/CMO superlattices, the relaxed strain state of the superlattices meant that the superlattice layers could reorient independently from one another, thus modulating the ferromagnetism. By modifying octahedral connectivity, we can stabilize crystal symmetries not observed in the bulk, thereby tuning interfacial magnetism.

In this paper, we show how octahedral connectivity can be used to stabilize nonequilibrium crystal symmetries that can suppress or enhance interfacial ferromagnetism in coherently strained $LaNiO_3/CaMnO_3$ $(LNO)_N/(CMO)_M$ superlattices. We establish that nonequilibrium crystal symmetries can be stabilized in superlattices composed of constituent materials with different bulk crystal symmetries. We find that different nonequilibrium crystal symmetries can be stabilized by varying the LNO and CMO layer thicknesses. In our superlattices, the magnitude of octahedral rotations in CMO is determined by the LNO layer thickness. However, the orientation of these octahedral rotations in CMO is controlled by the CMO layer thickness. Together, these structural modifications in LNO/CMO superlattices enable control of the interfacial ferromagnetic properties over a large range of magnitudes, leading to enhanced ferromagnetism. This demonstrates that octahedral connectivity is a promising path forward for engineering interfacial ferromagnetism at the nanoscale.

## II. EXPERIMENT

To this end, we studied $(LNO)_N/(CMO)_M$ superlattices on $5\,mm^2 \times 0.5\,mm$ (001) $LaAlO_3$ (LAO) single-crystal substrates, where $N$ and $M$ are the number of LNO unit cells and CMO unit cells per superlattice period, respectively. Two sets of superlattices were grown with $M$ equal to 4 and 8 unit cells (u.c.). For each $M$, $N$ was varied from 2 to 8. To maintain comparable overall thickness, $M = 4$ superlattice periods were repeated ten times, and $M = 8$ superlattice periods were repeated eight times. Films were deposited using a 248-nm KrF laser pulsed at 1 Hz with fluence of $1.3\,J/cm^2$.

 

The background pressure was 60 mTorr of $O_2$, and the substrate was heated to 700 °C. Unit-cell growth was monitored *in situ* via reflection high-energy electron diffraction (RHEED), for which intensity oscillations were observed for individual layers of each superlattice, indicating smooth layer-by-layer growth.

## III. STRUCTURE

Structural quality was characterized *ex situ* using x-ray reflectivity (XRR), x-ray diffraction (XRD), and atomic force microscopy (AFM) [14]. XRR [Fig. 1(b)] was performed at beamline 13-3 at the Stanford Synchrotron Radiation Lightsource. The 2θ-θ XRD scans [Fig. 1(c)] were performed at beamline 12ID-D at the Advanced Photon Source and indicate clear superlattice Bragg peaks and superlattice period thickness fringes. The visibility of total thickness fringes and superlattice Bragg peaks demonstrates high sample crystalline quality and layering. AFM of the superlattices reveals a surface roughness of less than a unit cell, consistent with the smooth growth of CMO and LNO at these conditions. Therefore XRR, XRD, and AFM all confirm high-quality and precise control of the superlattice growth in this study.

Reciprocal space maps of the (103) diffraction peaks reveal that both the CMO and LNO layers are coherently strained to the underlying LAO substrates in all of our superlattices. It is important to note that LAO forms a rhombohedral crystal lattice in the bulk with a pseudocubic lattice parameter of $a = 3.798$ Å. LNO also has a rhombohedral unit cell that can be approximated by a pseudocubic lattice parameter of $a = 3.85$ Å [15]. CMO has an orthorhombic unit cell that can be approximated by a pseudocubic lattice parameter of $a = 3.73$ Å [16]. In perovskite oxides, octahedral rotations are largely responsible for the various crystal symmetries that exist in compounds. For example, rhombohedral LNO has $a^-a^-a^-$ rotations, using Glazer notation [17]. In this notation a minus symbol refers to out-of-phase rotations while a plus symbol refers to in-phase rotations. On the other hand, CMO has $a^-a^-c^+$ rotations with in-phase rotations along the $c$ direction. Figure 1(a) illustrates the in-phase and out-of-phase rotations of these oxygen octahedra. Coherent strain therefore may impose a nonequilibrium unit cell and nonequilibrium octahedral rotations in the CMO and LNO layers depending on their relative thicknesses.

To probe how coherent strain modifies the CMO and LNO atomic structures in the superlattices, we examined half-order x-ray diffraction peaks at beamline 12ID-D of the Advanced Photon Source at Argonne National Laboratory. For perovskite oxides, differences in bond angles, bond lengths, and crystal symmetries can be described in terms of how the oxygen octahedra are rotated and tilted relative to one another; this is sometimes referred to as octahedral connectivity. This connectivity can be analyzed in terms of the existence and intensities of half-order diffraction peaks [17–19]. Here we examine (half half integer)-type peaks [e.g., (1/2 3/2 2)], which are uniquely associated with the in-phase rotation found only in CMO of these material constituents. The integer index corresponds to the axis of in-phase rotations [9,17,19]. The intensity of the half-order peaks is proportional to the magnitude of the rotation [9,17–20]. These diffraction peaks (Fig. 2), and therefore the associated structural accommodations, are distinctly different for the $M = 4$ and $M = 8$ superlattices, thereby affecting the interfacial ferromagnetism in different ways.

For $M = 4$ superlattices, Fig. 2(a) presents the evolution of the $(\frac{1}{2}\ \frac{3}{2}\ 2)$ half-order diffraction peak, which corresponds to the $c^+$-type, out-of-plane, in-phase rotation in CMO [9,17]. As the LNO thickness increases, the intensity of the in-phase rotations is reduced. It eventually disappears entirely by $N = 8$. We also found throughout all $M = 4$ samples that there are no in-plane, in-phase rotations associated with the $(0\ \frac{1}{2}\ \frac{3}{2})$ and $(\frac{1}{2}\ 0\ \frac{3}{2})$ peaks [dashed line in Fig. 2(b)]. Thus in the thin CMO regime, the growth axis is the preferred in-phase axis.

From these data, we can conclude that increasing the LNO layer thickness diminishes the out-of-plane, in-phase rotations in CMO, possibly imposing the LNO $a^-a^-a^-$ out-of-phase rotation pattern throughout the LNO and CMO layers of the superlattice. Unlike for in-phase rotations, there is no unique

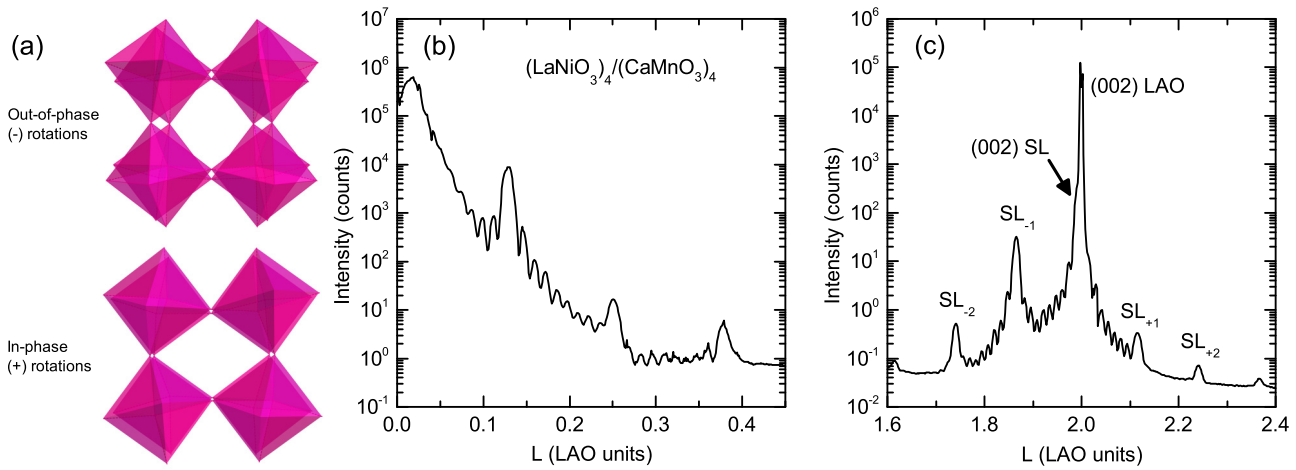


FIG. 1. (a) Schematics of out-of-phase rotations (top) and in-phase rotations (bottom). The direction of the rotation axis is into the paper. (b) Specular x-ray reflectometry scan showing typical reflectivity profile of a $N = 4$, $M = 4$ superlattice. The determination of the superlattice period via superlattice Bragg peaks agrees within 3% with the calculated value. (c) The $2\theta$-$\theta$ scan around the (002) $LaAlO_3$ (LAO) peak. Superlattice (SL) Bragg peaks and superlattice period thickness fringes are clearly seen, indicating high structural quality.

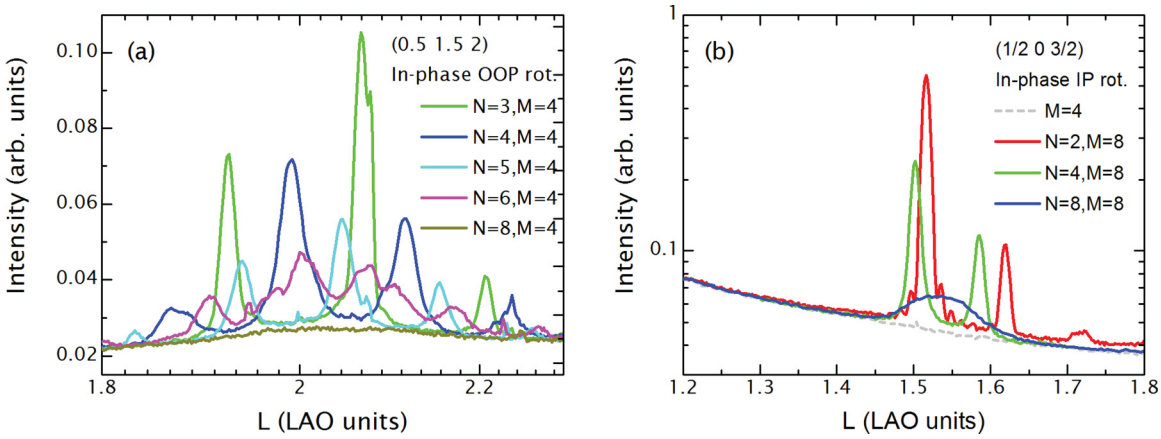


FIG. 2. (a) X-ray diffractogram of $(\frac{1}{2}\ \frac{3}{2}\ 2)$ half-order Bragg peak due to out-of-plane, in-phase rotations in CMO = 4 u.c. superlattices. As LNO layer thickness $N$ increases, in-phase CMO rotations decrease and eventually disappear. (b) X-ray diffractogram of $(\frac{1}{2}\ 0\ \frac{3}{2})$ half-order Bragg peak due to in-plane, in-phase rotations in CMO = 8 u.c. superlattices. As LNO layer thickness $N$ increases, in-phase CMO rotations decrease and nearly disappear by $N = 8$. The $M = 4$ superlattice (dashed line) is included to show the lack of in-phase IP rotations in $M = 4$ superlattices.

out-of-phase rotation half-order diffraction peak [17], and LAO and LNO both exhibit out-of-phase rotations. Therefore we cannot attribute a single-peak intensity to $a^-a^-a^-$ rotations in CMO using x-ray diffraction. As a result, it is not possible to definitively determine whether the LNO rhombohedral $a^-a^-a^-$ symmetry is established in the CMO or whether the CMO simply loses its in-phase rotations, resulting in $a^-a^-c^0$ rotations. At a minimum the in-phase rotations have been unrotated.

Changes in rotation pattern are accommodated via changes in Mn-O-Mn bond length as well as angle. This is due to the simple geometric relationship between the bond angle, rotation angle, and the resulting lattice constant [17,21]. As the out-of-plane, in-phase CMO rotations unrotate, the perpendicular in-plane bond angles must straighten. As a result, the Mn-Mn distance is now larger, thus increasing the unit-cell spacing. However, as confirmed via reciprocal space mapping, these superlattices are coherently strained to the substrate. Therefore the in-plane lattice constant is fixed. Hence straightening of the CMO in-plane bond angles must be accompanied by a corresponding shortening of the in-plane Mn-O bond lengths. A similar correlation between bond angle and bond length has been observed in LMO/STO superlattices [9]. These modifications to the Mn-O bond are expected to have significant consequences for the exchange interactions at the interface [6,9,22,23].

For $M = 8$ superlattices, we do not observe peaks at the $(\frac{1}{2}\ \frac{3}{2}\ 2)$ half-order diffraction index. Therefore, unlike $M = 4$ superlattices, $M = 8$ superlattices do not possess out-of-plane, in-phase rotations. By investigating $(0\ \frac{1}{2}\ \frac{3}{2})$- and $(\frac{1}{2}\ 0\ \frac{3}{2})$-type peaks, we find that the in-phase rotation axis of $M = 8$ superlattices is oriented in plane, with equal preference for the (1 0 0) [$(0\ \frac{1}{2}\ \frac{3}{2})$ half-order peak] and (0 1 0) [$(\frac{1}{2}\ 0\ \frac{3}{2})$ half-order peak] axes. This finding is consistent with the preferred orthorhombic growth direction observed in manganite thin films [24] and suggests that the stabilization of out-of-plane in-phase orientation for $M = 4$ superlattices may be a finite-size effect in the ultrathin regime. The evolution of the $(\frac{1}{2}\ 0\ \frac{3}{2})$ peak as a function of LNO layer thickness is shown in Fig. 2(b). For $M = 8$ superlattices, even though the CMO in-phase rotations are oriented in plane instead of out of plane, increasing $N$ has the same effect of straightening the in-phase rotations. By $N = 8, M = 8$, the in-phase rotations nearly have disappeared.

## IV. MAGNETISM

Bulk magnetization measurements revealed a ferromagnetic signal for all superlattices. Samples were measured at 10 K in fields up to 7 T using a superconducting quantum interference device magnetometer. Saturated magnetic moments for each superlattice are summarized in Fig. 3. The diamagnetic and paramagnetic substrate backgrounds were subtracted using linear and Brillouin functions,

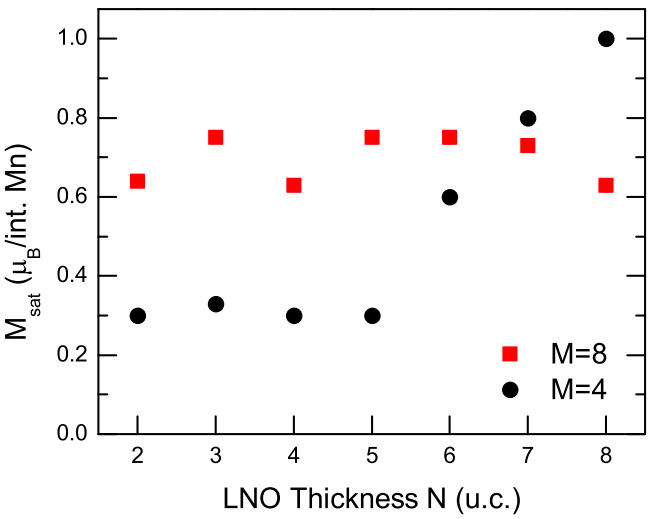


FIG. 3. LNO layer thickness dependence of the $(LNO)_N/(CMO)_M$ superlattice saturated magnetic moment at 7 T and 10 K. $(LNO)_N/(CMO)_4$ superlattices with $M = 4$ (black circles) exhibit a nearly constant $M_{sat}$ at low $N$ and increasing $M_{sat}$ with $N > 5$. Superlattices with $M = 8$ (red squares) exhibit a nearly constant $M_{sat}$ across the full range of LNO thicknesses.

respectively [25]. Furthermore, a small additional high-temperature ferromagnetic contribution was observed, which is consistent with previous studies on a commercially available perovskite oxide substrate [25–27]. This ferromagnetic contamination has been observed to be temperature independent below room temperature [25] and was subtracted from the saturated magnetic moment presented in Fig. 3. The saturated magnetic moment has been normalized to the number of interfacial Mn ions for comparison with previous work on CMO-based superlattices [13,28–31]. In light of the interesting finding of exchange bias in (111)-oriented LNO/LMO superlattices [32], we note that these samples do not exhibit exchange bias. This is not unexpected since CMO is a G-type antiferromagnet, and so along the (001) CMO planes, the Mn spins are fully compensated, in contrast to the (111) CMO planes, which are completely uncompensated.

Interfacial ferromagnetism in LNO/CMO has been explained by a double-exchange-based model of interfacial ferromagnetism in which a small number of electrons from the metallic LNO layer leak into the interfacial CMO layer and induce ferromagnetism [31,33]. In this scenario, the CMO layer determines the ferromagnetic properties via $Mn^{4+}$-$Mn^{3+}$ double exchange [33]. While the presence of ferromagnetism in metallic superlattices is consistent with the electron-leakage scenario [31,33,34], there are two features in our $M = 4$ and $M = 8$ samples that are unexplained by this model alone: (1) at low $N$ ($N \leqslant 4$), $M = 8$ superlattices have approximately double the saturated magnetic moment of the $M = 4$ superlattices, and (2) at large $N$ ($N > 5$), the saturated magnetic moment of $M = 8$ superlattices is constant, while the saturated magnetic moment of the $M = 4$ superlattices strongly depends on the LNO layer thicknesses. These results contrast with previous studies of electron-leakage-based interfacial ferromagnetism, in which the magnitude of the interfacial ferromagnetism was found to be constant with thickness variations [28,30].

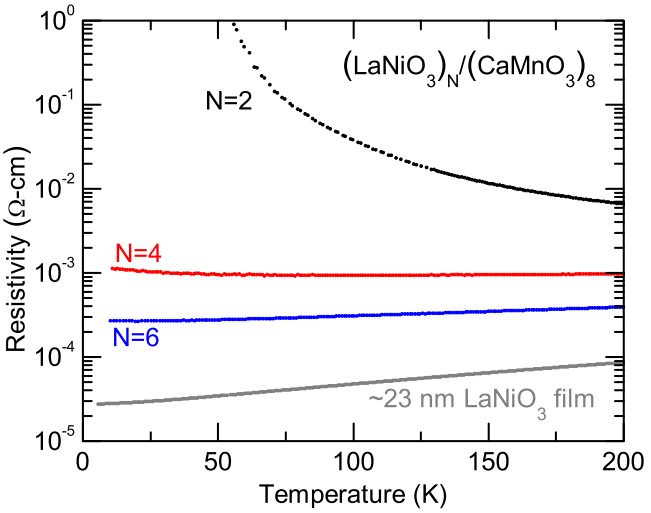


FIG. 4. Temperature dependence from 10 to 200 K of superlattice resistivity for $M = 8$, $N = 2,4,6$ superlattices. Included is temperature dependence from 5 to 200 K of LNO thin-film resistivity for comparison. A metal-insulator transition at $N = 4$ with minima in ultrathin metallic films and a gradual approach to bulk LNO value are observed, consistent with previous results [31,35].

Since the interfacial double-exchange model depends on electronic properties of the LNO layer, we performed electronic transport measurements to characterize the superlattice conductivity. Figure 4 shows resistivity versus temperature of $M = 8$, $N = 2,4,6$ superlattices from 5 to 200 K. A 23-nm-thick film of LNO grown under the same conditions is provided for comparison. $M = 4$ superlattices are omitted for clarity but show a similar trend. For $M = 4$ and $M = 8$ superlattices, there is a metal-insulator transition at $N = 4$ unit cells, with $N \geqslant 4$ superlattices being metallic, albeit with a low-temperature minimum consistent with previous $LaNiO_3$ thin films [35]. While all superlattices with $N < 4$ are insulating, they are still magnetic [36]. This means that at low $N$, an additional interfacial ferromagnetic mechanism must be operative. The most likely mechanism is a Ni-O-Mn superexchange interaction that we have described in more detail elsewhere [34]. Since the $M = 4$ and $M = 8$ superlattices have similar resistivity behaviors, the transport data do not explain the difference in magnetic moment between $M = 4$ and $M = 8$ superlattices at low $N$, nor does it explain the difference in magnetic moment trends as a function of LNO layer thickness.

## V. DISCUSSION

We must therefore turn to alternative explanations for the observed ferromagnetism. Given the evolution of the structural data as a function of $N$ for $M = 4$, a closer look at the relationship between structural and magnetic properties in these superlattices is warranted. We propose a model based on tuning octahedral rotations that depends on the interfacial alignment between LNO and CMO. Figure 5(a) illustrates this alignment and the differences between $M = 4$ and $M = 8$ superlattices. In addition to the magnetization data, Figs. 5(b) and 5(c) depict the x-ray intensity of the in-phase rotation peaks with a calculated line that assumes a constant change $\delta$ in the in-phase rotation angle for each additional LNO unit cell added to the superlattice. With respect to the influence of the octahedral rotations on the trend of magnetization, it is most important to consider relative changes in the rotation angles rather than absolute angles, which require extensive measurements and may not have the accuracy needed to examine layer-by-layer changes [19]. Utilizing BIOVIA MATERIALS STUDIO [37], we use a model in which the in-phase rotation angle starts at some initial value and changes linearly with LNO layer thickness; that is, each additional LNO layer reduces the in-phase rotation angle by an amount $\delta$. We now discuss the correlation between these x-ray data and the magnetization data in more depth.

For $M = 4$ superlattices, as the thickness of the LNO metallic layer is increased from $N = 5$ to $N = 8$, the saturated moment per interfacial Mn shows a drastic increase (i.e., more than triples). In CRO/CMO, the saturated magnetic moment has been found to be constant with thickness [28,30]. Consequently, even though double-exchange ferromagnetism exists in the metallic superlattices, the increasing saturated magnetic moment is not sufficiently explained merely by the existence of interfacial itinerant electron-based double-exchange interaction due to the adjacent metallic layer. As mentioned previously, it is known for perovskite oxides that changes in octahedral rotations modify the $B$-O-$B$ bond angles

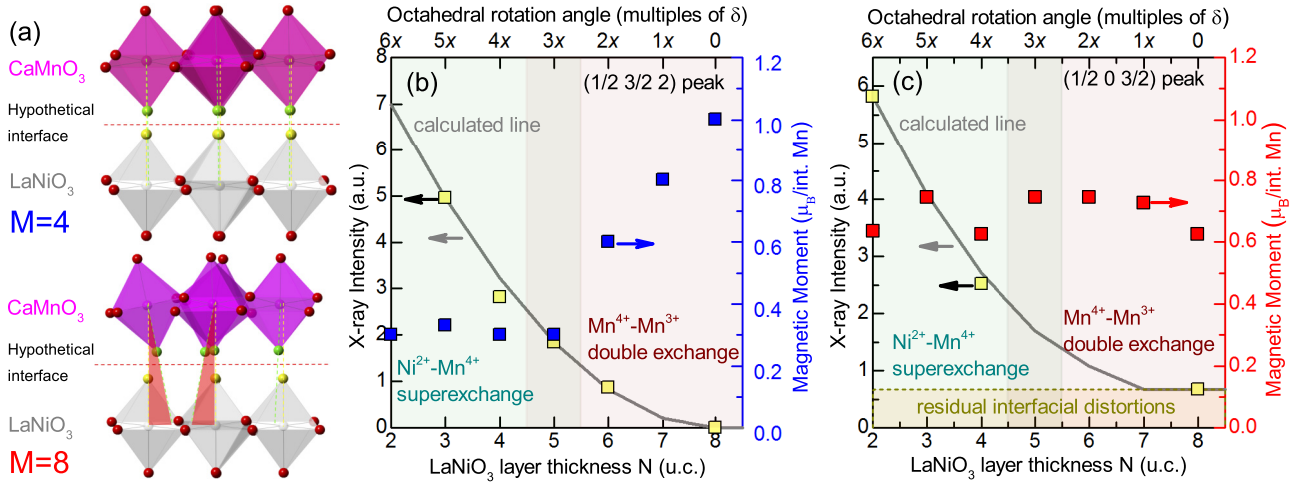


FIG. 5. (a) Hypothetical interfacial alignment for $M = 4$ and $M = 8$ superlattices demonstrating $M = 8$ mismatch due to in-plane orthorhombic orientation. (b) X-ray intensity of the $(\frac{1}{2}\ \frac{3}{2}\ 2)$ half-order Bragg peak due to out-of-plane, in-phase rotations in CMO = 4 u.c. superlattices (left axis). As LNO layer thickness $N$ increases, in-phase CMO rotations decrease and eventually disappear. The calculated line shows the expected intensity for a constant decrease in the rotation angle with increasing LNO layer thickness. Saturated magnetic moment (right axis) increases once the double-exchange interaction is dominant. (b) X-ray intensity of the $(\frac{1}{2}\ 0\ \frac{3}{2})$ half-order Bragg peak due to in-plane, in-phase rotations in CMO = 8 u.c. superlattices (left axis). As LNO layer thickness $N$ increases, in-phase CMO rotations decrease and nearly disappear by $N = 8$. The calculated line shows the experimental data are well fit to the same model as $M = 4$, with the addition of a constant intensity offset due to interfacial mismatch.

and bond lengths and that these effects can impact the magnetic properties. Within this context, a possible explanation for the observed magnetic trend is enhancement of the interfacial double-exchange mechanism as a result of the stabilization of nonequilibrium crystal symmetries. The modification of the CMO symmetry to reduce the orthorhombic distortion may enhance the interfacial double-exchange mechanism. One possible reason for this modification is the influence of biaxial strain from the LAO substrate, which leads to a monoclinic distortion in bulk LNO with out-of-plane rotations that are much larger than the in-plane rotations [18]. On the other hand, epitaxially strained CMO on LAO is predicted to have large in-plane and out-of-plane rotations [21]. As the LNO thickness increases and CMO adopts the $a^-a^-c^0$ pattern, the out-of-plane, in-phase rotation angle is reduced. Reducing the out-of-plane rotation angle has the effect of increasing the in-plane $B$-O-$B$ bond angle [17,20]. Increasing the in-plane Mn-O-Mn bond angles would enhance the double-exchange interaction between $Mn^{4+}$ and $Mn^{3+}$ ions [9,23]. This symmetry change in the CMO layer can be easily accommodated across the interface because changes to the out-of-plane rotations affect the in-plane rotation angles.

In addition to explaining the trend of increasing magnetization at $N > 5$, the symmetry change from $a^-a^-c^+$ to $a^-a^-c^0$ is also consistent with constant magnetization in $N = 2$–5 superlattices. Changes to the out-of-plane rotations from increasing LNO layer thickness do not strongly influence the apical oxygens across the LNO-CMO interface. Only rotation angles perpendicular to the rotation axes (i.e., in-plane rotation angles) are affected. Since the rotations along the out-of-plane axis are able to freely rotate, leaving the apical oxygens undisturbed, the dominant mechanism at low $N$ (Ni-O-Mn superexchange across the interface) is unaffected.

However, turning to the $M = 8$ superlattices, one observes that the LNO layer thickness has little influence on the magnetic moment. In other words, even though the LNO layer leads to a similar reduction in the CMO in-phase rotation, it does not result in a similar increase in magnetic moment. This suggests that while the crystal symmetry control via LNO layer thickness is important for determining magnetic properties, it depends critically on the CMO orthorhombic orientation, which is determined by the CMO layer thickness. In $M = 8$ superlattices, the CMO orthorhombic axis is in plane, which means reductions in the in-phase rotations should directly affect the interfacial apical oxygens. In these superlattices, one may expect changes in the in-phase rotations in CMO to modify the Ni-O-Mn bond angle. However, since no change is observed in the saturated magnetic moment of these samples, the superexchange and double-exchange mechanisms must be unaffected. Thus the interface Ni-O-Mn and Mn-O-Mn bond angles are similarly unaffected.

One possible scenario then is that the CMO interface maintains a constant and distinct rotation pattern from the interior of the CMO layer. Constant and distinct interfacial distortions previously have been observed in $La_{0.67}Sr_{0.33}MnO_3$ and $SrRuO_3$ thin films [38,39]. As the majority of the CMO unrotates with increasing LNO layer thickness, the interface maintains its structural state. For the x-ray intensity in Fig. 5(c), this would be the equivalent to a constant offset in the modulation of the x-ray intensity with LNO thickness. Indeed, from Fig. 5(c) we find that the x-ray data for $M = 8$ superlattices matches well with this model. These results suggest that in the $M = 8$ superlattices, the interface may adopt a distinct structural state, separate from the CMO and LNO rotation patterns. Interfacial octahedral distortions are associated with the apical oxygen locations [39]. From Fig. 5(a), it is clear that there is a mismatch in the preferred apical oxygen

locations across the $M = 8$ LNO/CMO interface that is not present in the $M = 4$ LNO/CMO interface. The apical oxygen mismatch in $M = 8$ superlattices arises from the crystal symmetry mismatch at this interface and leads to the distorted interface. This intermediate interfacial state, arising from the in-plane CMO orthorhombic orientation ($M = 8$ superlattices), results in lower tunability of the ferromagnetism within this LNO thickness range compared to that arising from the out-of-plane CMO orthorhombic orientation ($M = 4$ superlattices). However, this interfacial state in $M = 8$ superlattices also leads to a higher saturated magnetic moment at low $N$.

The dependence of the magnetic moment evolution on the orientation of the CMO in-phase rotation axis (out of plane for $M = 4$ and in plane for $M = 8$) suggests that the transition from $a^-a^-c^+$ to $a^-a^-c^0$ may be accommodated differently than the transition from $a^-c^+a^-$ or $c^+a^-a^-$ to $a^-c^0a^-$ or $c^0a^-a^-$, respectively. In fact, modulations in magnetization at symmetry-mismatched interfaces have previously been observed in CRO/CMO superlattices [13]. These results suggest that symmetry mismatch may be a more general method for manipulating interfacial ferromagnetism. Further studies are needed to understand exactly how the interface accommodates the transition from CMO-type rotations to LNO-type rotations. One critical tuning parameter may be the $N/M$ ratio. For $M = 4$ superlattices, the increase in magnetization is not observed until $N/M = 3/2$, while for $M = 8$ superlattices, we investigated only up to $N/M = 1$. In this thickness regime, while Fig. 2(b) demonstrates that the intensity of the CMO in-phase rotation in $M = 8$ superlattices is nearly diminished by $N = 8$, a small, broad peak is still apparent. It is clear from a comparison of the XRD intensities that the $M = 8$ CMO in-phase rotations are much more strongly diminished by $N/M = 1$ than those in the $M = 4$ case. However, this remnant intensity supports the assertion that the CMO rotations for $M = 8$ and $N = 8$ are in some intermediate state due to difficulty in accommodating changes in phase and magnitude of the in-plane $c^+$ rotation.

## VI. SUMMARY

By investigating superlattices with 4 and 8 u.c. of CMO across a range of LNO layer thicknesses, we have demonstrated that the stabilization of nonequilibrium crystal symmetries of a material via heteroepitaxy can give rise to a wide range of interfacial ferromagnetic responses via octahedral connectivity. We find that the LNO thickness controls the magnitude of the CMO in-phase rotations, and the CMO thickness determines the rotation orientation. Moreover, LNO layer thicknesses approaching 8 u.c. suppress the orthorhombic symmetry of the CMO layers. Our studies indicate that differences in the emergent ferromagnetic behavior of superlattices with 4 and 8 u.c. of CMO are the result of how the anisotropic octahedral rotations influence the strength of the anisotropic ferromagnetic exchange interactions at the LNO-CMO interface and demonstrate the complex interplay of in-phase and out-of-phase rotations on the functional properties. This understanding of the relationship between crystal symmetry and interfacial ferromagnetism is important for the future development of oxide-based electronics and spintronics.

## ACKNOWLEDGMENTS

Research was supported by the U.S. Department of Energy, Director, Office of Science, Office of Basic Energy Sciences, Division of Materials Sciences and Engineering, under Contract No. DESC0008505. Use of the Stanford Synchrotron Radiation Light source, SLAC National Accelerator Laboratory, is supported by the U.S. Department of Energy, Office of Science, Office of Basic Energy Sciences, under Contract No. DE-AC02-76SF00515. The Advanced Light Source is supported by the Director, Office of Science, Office of Basic Energy Sciences, of the U.S. Department of Energy under Contract No. DE-AC02-05CH11231. Use of the Advanced Photon Source was supported by the U.S. Department of Energy, Office of Science, Office of Basic Energy Sciences, under Contract No. DE-AC02-06CH11357.

[1] V. Laukhin, J. Fontcuberta, J. L. García-Muñoz, and X. Obradors, Phys. Rev. B **56**, R10009 (1997).
[2] T. Vogt, J. A. Hriljac, N. C. Hyatt, and P. Woodward, Phys. Rev. B **67**, 140401 (2003).
[3] T. Kawakami and S. Nasu, J. Phys. Condens. Matter **17**, S789 (2005).
[4] A. Y. Ramos, N. M. Souza-Neto, H. C. N. Tolentino, O. Bunau, Y. Joly, S. Grenier, J.-P. Iti, A.-M. Flank, P. Lagarde, and A. Caneiro, Europhys. Lett. **96**, 36002 (2011).
[5] I. Fita, R. Puzniak, A. Wisniewski, V. Markovich, I. O. Troyanchuk, and Y. G. Pashkevich, J. Appl. Phys. **114**, 153910 (2013). .
[6] J. M. Rondinelli, S. J. May, and J. W. Freeland, MRS Bull. **37**, 261 (2012).
[7] J. He, A. Borisevich, S. V. Kalinin, S. J. Pennycook, and S. T. Pantelides, Phys. Rev. Lett. **105**, 227203 (2010).
[8] J. M. Rondinelli and C. J. Fennie, Adv. Mater. **24**, 1918 (2012).
[9] X. Zhai, L. Cheng, Y. Liu, C. M. Schlepütz, S. Dong, H. Li, X. Zhang, S. Chu, L. Zheng, J. Zhang, A. Zhao, H. Hong, A. Bhattacharya, J. N. Eckstein, and C. Zeng, Nat. Commun. **5**, 4283 (2014).
[10] E. J. Moon, R. Colby, Q. Wang, E. Karapetrova, C. M. Schlepütz, M. R. Fitzsimmons, and S. J. May, Nat. Commun. **5**, 5710 (2014).
[11] E. J. Moon, P. V. Balachandran, B. J. Kirby, D. J. Keavney, R. J. Sichel-Tissot, C. M. Schleptz, E. Karapetrova, X. M. Cheng, J. M. Rondinelli, and S. J. May, Nano Lett. **14**, 2509 (2014).
[12] Z. Liao, M. Huijben, Z. Zhong, N. Gauquelin, S. Macke, R. Green, S. Van Aert, J. Verbeeck, G. Van Tendeloo, K. Held, G. Sawatzky, G. Koster, and G. Rijnders, Nat. Mater. **15**, 425 (2016).
[13] A. J. Grutter, A. Vailionis, J. A. Borchers, B. J. Kirby, C. L. Flint, C. He, E. Arenholz, and Y. Suzuki, Nano Lett. **16**, 5647 (2016).

[14] See Supplemental Material at http://link.aps.org/supplemental/10.1103/PhysRevB.96.144438 for atomic force microscopy, additional x-ray reflectivity, and reciprocal space mapping.
[15] K. Sreedhar, J. M. Honig, M. Darwin, M. McElfresh, P. M. Shand, J. Xu, B. C. Crooker, and J. Spalek, Phys. Rev. B **46**, 6382 (1992).
[16] W. Paszkowicz, J. Pitosa, S. M. Woodley, P. A. Duewski, M. Kozowski, and C. Martin, Powder Diffr. **25**, 46 (2012).
[17] A. M. Glazer, Acta Crystallogr., Sect. A **31**, 756 (1975).
[18] S. J. May, J.-W. Kim, J. M. Rondinelli, E. Karapetrova, N. A. Spaldin, A. Bhattacharya, and P. J. Ryan, Phys. Rev. B **82**, 014110 (2010).
[19] M. Brahlek, A. K. Choquette, C. R. Smith, R. Engel-Herbert, and S. J. May, J. Appl. Phys. **121**, 045303 (2017).
[20] S. J. May, C. R. Smith, J.-W. Kim, E. Karapetrova, A. Bhattacharya, and P. J. Ryan, Phys. Rev. B **83**, 153411 (2011).
[21] U. Aschauer, R. Pfenninger, S. M. Selbach, T. Grande, and N. A. Spaldin, Phys. Rev. B **88**, 054111 (2013).
[22] G. Sawatzky, W. Geertsma, and C. Haas, J. Magn. Magn. Mater. **3**, 37 (1976).
[23] H. Y. Hwang, S.-W. Cheong, P. G. Radaelli, M. Marezio, and B. Batlogg, Phys. Rev. Lett. **75**, 914 (1995).
[24] A. Vailionis, H. Boschker, W. Siemons, E. P. Houwman, D. H. A. Blank, G. Rijnders, and G. Koster, Phys. Rev. B **83**, 064101 (2011).
[25] M. Khalid, A. Setzer, M. Ziese, P. Esquinazi, D. Spemann, A. Pöppl, and E. Goering, Phys. Rev. B **81**, 214414 (2010).
[26] F. Golmar, A. M. M. Navarro, C. E. R. Torres, F. H. Snchez, F. D. Saccone, P. C. dos Santos Claro, G. A. Bentez, and P. L. Schilardi, Appl. Phys. Lett. **92**, 262503 (2008).
[27] S. M. M. Yee, D. A. Crandles, and L. V. Goncharova, J. Appl. Phys. **110**, 033906 (2011).
[28] K. S. Takahashi, M. Kawasaki, and Y. Tokura, Appl. Phys. Lett. **79**, 1324 (2001).
[29] J. W. Freeland, J. Chakhalian, A. V. Boris, J.-M. Tonnerre, J. J. Kavich, P. Yordanov, S. Grenier, P. Zschack, E. Karapetrova, P. Popovich, H. N. Lee, and B. Keimer, Phys. Rev. B **81**, 094414 (2010).
[30] C. He, A. J. Grutter, M. Gu, N. D. Browning, Y. Takamura, B. J. Kirby, J. A. Borchers, J. W. Kim, M. R. Fitzsimmons, X. Zhai, V. V. Mehta, F. J. Wong, and Y. Suzuki, Phys. Rev. Lett. **109**, 197202 (2012).
[31] A. J. Grutter, H. Yang, B. J. Kirby, M. R. Fitzsimmons, J. A. Aguiar, N. D. Browning, C. A. Jenkins, E. Arenholz, V. V. Mehta, U. S. Alaan, and Y. Suzuki, Phys. Rev. Lett. **111**, 087202 (2013).
[32] M. Gibert, P. Zubko, R. Scherwitzl, J. Íñiguez, and J.-M. Triscone, Nat. Mater. **11**, 195 (2012).
[33] B. R. K. Nanda, S. Satpathy, and M. S. Springborg, Phys. Rev. Lett. **98**, 216804 (2007).
[34] C. L. Flint, H. Jang, J.-S. Lee, A. T. N'Diaye, P. Shafer, E. Arenholz, and Y. Suzuki, Phys. Rev. Mater. **1**, 024404 (2017).
[35] R. Scherwitzl, S. Gariglio, M. Gabay, P. Zubko, M. Gibert, and J.-M. Triscone, Phys. Rev. Lett. **106**, 246403 (2011).
[36] It should be noted that in a previous study, no ferromagnetism was observed in $M = 8$ insulating superlattices [31]. A careful comparison of the transport data of the $M = 8$ superlattices in this current study to those of the previous study reveals that the present superlattices have higher resistivity at a given $N$ and $M$. These differences in resistivity suggest there may be differences in oxygen stoichiometry and cation oxidation states at the interface between sample sets. These differences are plausible given the different growth conditions.
[37] Dassault Systèmes BIOVIA, BIOVIA MATERIALS STUDIO, version 8, Dassault Systèmes, San Diego, 2015.
[38] A. Vailionis, H. Boschker, Z. Liao, J. R. A. Smit, G. Rijnders, M. Huijben, and G. Koster, Appl. Phys. Lett. **105**, 131906 (2014).
[39] R. Aso, D. Kan, Y. Shimakawa, and H. Kurata, Sci. Rep. **3** (2013).